

# Parameter Estimation in an SPDE Model for Cell Repolarisation\*

Randolf Altmeyer<sup>†</sup>   Till Bretschneider<sup>‡</sup>   Josef Janák<sup>§</sup>   Markus Reiß<sup>¶</sup>

January 7, 2022

## Abstract

As a concrete setting where stochastic partial differential equations (SPDEs) are able to model real phenomena, we propose a stochastic Meinhardt model for cell repolarisation and study how parameter estimation techniques developed for simple linear SPDE models apply in this situation. We establish the existence of mild SPDE solutions and we investigate the impact of the driving noise process on pattern formation in the solution. We then pursue estimation of the diffusion term and show asymptotic normality for our estimator as the space resolution becomes finer. The finite sample performance is investigated for synthetic and real data resembling experimental findings for cell orientation.

## 1 Introduction

Stochastic partial differential equations (SPDEs) generalize deterministic partial differential equations (PDEs) by introducing driving noise processes into the dynamics. These noise processes encapsulate unresolved and often unknown processes happening at faster scales and random external forces acting on the system. Not only the theory of SPDEs, but also the statistics for SPDEs have recently seen a significant development, paving the way for a realistic modeling of complex phenomena. We demonstrate the ability of SPDE models

---

\*This research has been partially funded by Deutsche Forschungsgemeinschaft (DFG) - SFB1294/1 - 318763901. RA gratefully acknowledges support by the European Research Council, ERC grant agreement 647812 (UQMSI).

<sup>†</sup>University of Cambridge, Department of Pure Mathematics & Mathematical Statistics, Wilberforce Road, CB3 0WB Cambridge, United Kingdom. Email: ra591@cam.ac.uk.

<sup>‡</sup>Department of Computer Science, University of Warwick, Academic Loop Road, CV4 7AL Coventry, United Kingdom. Email: T.Bretschneider@warwick.ac.uk.

<sup>§</sup>Universität Potsdam, Institut für Mathematik, Karl-Liebknecht-Str. 24/25, 14476 Potsdam, Germany. Email: josefjanak@seznam.cz.

<sup>¶</sup>Humboldt-Universität zu Berlin, Institut für Mathematik, Unter den Linden 6, 10099 Berlin, Germany. Email: mreiss@math.hu-berlin.de.

to describe cell repolarisation patterns and we show how parameter estimation techniques, developed for simplified linear models, apply in more complex and physically relevant situations. We see this as an important step to make theoretical tools also available for concrete experimental setups. For the sake of clarity we focus on a specific stochastic cell polarisation problem, but the methodology has a much broader scope.

The SPDE we are interested in belongs to a general class of activator-inhibitor models, which can be described by two coupled stochastic reaction-diffusion equations  $X = (A, I)$  of the form

$$\begin{cases} \frac{\partial}{\partial t} A(t, x) = D_A \frac{\partial^2}{\partial x^2} A(t, x) + f_A(X(t, x), x) + \sigma_A \xi_A(t, x), \\ \frac{\partial}{\partial t} I(t, x) = D_I \frac{\partial^2}{\partial x^2} I(t, x) + f_I(X(t, x), x) + \sigma_I \xi_I(t, x), \end{cases} \quad (1)$$

where  $X = (A, I)$ , with nonlinear functions  $f_A, f_I$  and with space-time white noise processes  $\xi_A, \xi_I$ . In cell dynamics, we think of  $A$  as a hypothetical signalling molecule that in response to an external signal gradient becomes enriched on one side of the cell, yielding polarity.  $I$  counter-acts  $A$  so that removal of the signal results in loss of polarity. We here specifically consider repolarisation, where the extracellular signal gradient is inverted so that  $A$  is removed from one side of the cell and reappears on the opposite side, cf. Figure 1 below.

In directed animal cell motion cells respond to for example chemical or mechanical extracellular signal gradients by adopting a functional asymmetry in form of a front-rear pattern. Protrusion of the cell front is driven by local oriented growth of a dense network of cytoskeletal actin filaments pushing the cellular envelope [29]. Myosin-II motor molecules contracting the looser, ubiquitous cortical actin network lining the cell membrane result in retraction of the cell rear in stringent environments [11].

Models for spontaneous symmetry breaking in non-linear reaction diffusion systems by Turing [35] have been instrumental in understanding biological pattern formation, often paraphrased in form of simple deterministic two-variable activator-inhibitor models such as (1) without noise terms. Suprathreshold random perturbations can result in fast autocatalytic local growth of the activator variable  $A$ , which eventually is kept in check by the slower inhibitor  $I$ . Faster diffusion of the inhibitor compared to the activator prevents formation of nearby activator peaks.

Meinhardt [27] has been the first to apply such models to cell polarisation in the context of cell migration, where the ratio of activator-inhibitor diffusion can be tuned to either obtain a single stable cell front (Figure 1(center)), or multiple independent fronts associated with non-directed random cell motility. Various mathematical models for cell polarisation and gradient sensing have been postulated ([22], [30], [20]) aiming to capture different aspects of cellular physiology for example with regards to adaptation to extracellular signals, reviewed in [6]. [25] fitted deterministic versions of three different models for cell polarisation to experimental data of cells in a microfluidic chamber responding to inversion of gradients of hydrodynamic shear flow of different strengths [13]. The parameter calibration was based on a least-squares approach, implicitly assuming that the deterministic dynamics are corrupted by Gaussian measurement noise.

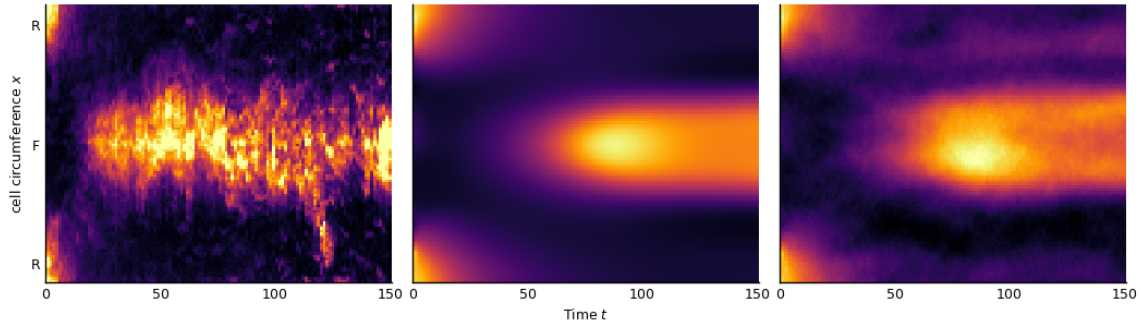


**Figure 1:** Heat maps for the space-time evolution of the activator  $A$ , brighter colors mean higher values, space region R denotes the old front/new rear, region F is the new front/old rear; (left) experimental data for measured fluorescence values averaged over several *Dictyostelium* cells reacting to a gradient of shear flow; (center) solution to the deterministic Meinhardt model with experimentally fitted parameters; (right) a typical realisation of the stochastic Meinhardt model with noise level 0.02.

Recognising that in confined spaces and with limited number of molecules noise becomes increasingly important, more recently stochastic reaction-diffusion models for different biological problems have been employed, e.g. in [1], [33]. Spontaneous symmetry breaking in Turing-type models requires initial random perturbations, but we expect dynamic noise to destabilise patterns if the power of the noise is too large.

In the current paper we present a stochastic version of the modified Meinhardt two-variable model [25]. We believe that the stochasticity in the data is to some considerable extent due to dynamic noise entering the dynamics as in (1). The data generated from such a stochastic Meinhardt model is qualitatively of a different nature compared to a deterministic PDE model corrupted by measurement errors. We perform a systematic study of the effect of different noise levels on the repolarisation of cells. One result is that inclusion of moderate levels of noise in the model speeds up the repolarisation of cells, which biologically is interesting because it seems to be against our intuition that noise would negatively interfere with the formation of a pattern.

Recently, new tools for parameter estimation of stochastic differential equations have been developed, see [8] for an overview. Most approaches focus on estimating coefficients for the linear part of the equation, either from discrete [9], [17] or spectral [18], [32] observations, but also aspects of the driving noise have been analysed [7], [5]. Owing to the physical restriction of being able to measure only local averages, [3] have introduced local measurements and constructed estimators in a linear SPDE for the diffusion term which are provably rate-optimal. Even more, the proposed estimators apply in a nonparametric setting of spatially varying diffusion and are robust to misspecification of the noise or when subject to certain nonlinearities [2].

We extend the estimation method in [3] to cope also with multiple spatial measure-

ments, systems of SPDEs as (1) and with more general boundary conditions (here periodic boundary conditions will apply), cf. Remark 3. We shall perform parameter estimation in the stochastic Meinhardt model for cell repolarisation and provide confidence intervals to quantify the uncertainty. In particular, we are interested in determining the diffusion constant for the activator in the Meinhardt model. Although the activator variable in the model cannot be directly related to a specific molecular component, putting limits on how fast the activator spreads can ideally help narrowing down possible mechanisms. For example, spreading of the activator could be down to lateral growth of the actin network (slow), diffusion of chemoattractant receptors within the cell membrane (medium) or diffusion of phospholipid signalling molecules (PIP3) within the cell membrane (fast).

Mathematically, we derive a central limit theorem for our estimator by using advanced tools from stochastic analysis and semigroup theory. We are aware of only one related work [31], which uses the spectral method to fit parameters of a 2D Fitz-Hugh-Nagumo model for travelling actin waves through cells. For the stochastic Meinhardt model we compare in Section 5 below our method with the spectral estimation method.

In the next Section 2 the stochastic Meinhardt model is introduced, along with a rigorous proof for existence of a solution. Section 3 presents the main insights how adding noise to the Meinhardt model affects the dynamics and repolarisation. In Section 4 estimators for local measurements of the activator are analysed mathematically and applied in Section 5 to synthetic data, and in Section 6 to experimental data. Section 7 discusses the main results. All technical details and proofs are deferred to Appendix A. A description of the setup for numerical experiments and real data can be found in Appendix B.

## 2 The stochastic Meinhardt model

Diffusion is considered to take place along the cell contour, and so we study the equation (1) for  $t \geq 0$  on a circle or 1D-torus  $\Lambda = \mathbb{R}/(L\mathbb{Z})$  of length  $L > 0$  or, equivalently, on  $\Lambda = [0, L]$  with periodic boundary conditions.  $A$  describes a membrane-bound autocatalytic activator requiring  $f_A$  to be nonlinear, and with diffusion coefficient  $D_A$ . The production of  $A$  is counteracted by a small cytosolic inhibitor  $I$  with faster diffusion (that is,  $D_I > D_A$ ), where  $f_I$  is linear or nonlinear. In case of the two-variable Meinhardt model the functions  $f_A$  and  $f_I$  are given by

$$f_A(y, x) = r_A \frac{\zeta(x) (b_A + y_1^2)}{(\zeta_I + |y|) (1 + \zeta_A y_1^2)} - r_A y_1, \quad f_I(y, x) = b_I y_1 - r_I y_2, \quad (2)$$

for  $y \in \mathbb{R}^2$  and  $x \in \Lambda$ . The function

$$\zeta(x) = 1 + a \cdot \cos(2\pi(x/L + 1/2)) \quad (3)$$

corresponds to an extracellular signal, for example a gradient of chemoattractant, which stimulates the production of  $A$  with signal strength modulated by a constant  $a$ . The constants  $r_A$ ,  $r_I$  and  $b_A$ ,  $b_I$  are degradation and production rates,  $\zeta_A$  controls the saturation

and the Michaelis-Menten constant  $\zeta_I$  prevents  $f_A$  from exploding. While  $b_I$  is fixed in our setup, it will generally depend on the pressure of the signal  $\zeta$  [25]. For a more detailed description of the nonlinearities  $f_A$ ,  $f_I$  and a stability analysis for varying parameters see [24], [28].

Additional external forces acting on the cell membrane are modeled by two independent space-time white noise processes  $\xi_A$ ,  $\xi_I$ . By space-time white noise we mean a centered Gaussian process  $\xi$  on  $[0, T] \times \Lambda$  with covariance function

$$\text{Cov}(\xi(t, x), \xi(t', x')) = \delta(t - t')\delta(x - x').$$

By integrating formally against test functions,  $\xi$  induces an isonormal Gaussian process on  $L^2([0, T] \times \Lambda)$ . In this way, space-time white noise corresponds to a random Schwartz distribution on  $L^2(\Lambda)$  with values in negative Sobolev spaces [16]. Since the nonlinearity  $f_A(X(t, x), x)$  is not well-defined for a distribution valued process  $X$ , this means we cannot obtain classical solutions to the SPDE (1). After formally integrating the noise, however,  $W(t) = \int_0^t \xi(s, \cdot) ds$  is a (cylindrical) Wiener process with values in  $L^2(\Lambda)$  [12], and we can use the well-developed theory for SPDEs to show that (1) is well-posed in the mild sense. The solution even has some minimal spatial regularity.

**Theorem 1.** *Consider the stochastic Meinhardt model corresponding to the SPDE in (1) with nonlinearities  $f_A$ ,  $f_I$  from (2) on  $\Lambda = \mathbb{R}/(L\mathbb{Z})$ . Assume for the initial value  $(A_0, I_0) \in C^{2+s}(\Lambda; \mathbb{R}^2)$  for  $0 < s < 1/2$ . Then there exists a unique mild solution  $X = (A, I) \in C([0, T]; C^s(\Lambda; \mathbb{R}^2))$ . The solution can be decomposed as  $X = \bar{X} + \tilde{X}$ , where  $\bar{X}$  solves the linear equation (1) with  $f_A = f_I = 0$  and zero initial value, and with a perturbation process  $\tilde{X} \in C([0, T]; C^{2+s}(\Lambda; \mathbb{R}^2))$ .*

For the proof in Appendix A.1 we shall employ the language of stochastic analysis, while for modeling purposes we prefer (1) with the physical white noise interpretation. A more realistic model might consider multiplicative noise levels  $\sigma_A$ ,  $\sigma_I$  depending on  $X$ . Moreover, also the parameters and initial conditions could be subject to noise [20]. Here, we refrain from this generality and focus on the impact of simple additive space-time white noise in (1). Note that neither the model proposed by Meinhardt nor other models suggested in the literature for cell repolarisation include dynamic noise so far.

### 3 The effect of noise

In Turing-type models for pattern formation noise in the initial condition is required to leave a homogeneous steady state. Its strength determines how fast a suprathreshold level for the activator  $A$  starts growing into a pattern whose wavelength can be determined by linear stability analysis. Dynamic noise, on the other hand, is expected to destabilise this pattern either over time, or very suddenly. Contrary to this intuition, we will now describe two noteworthy effects arising from moderate noise levels.

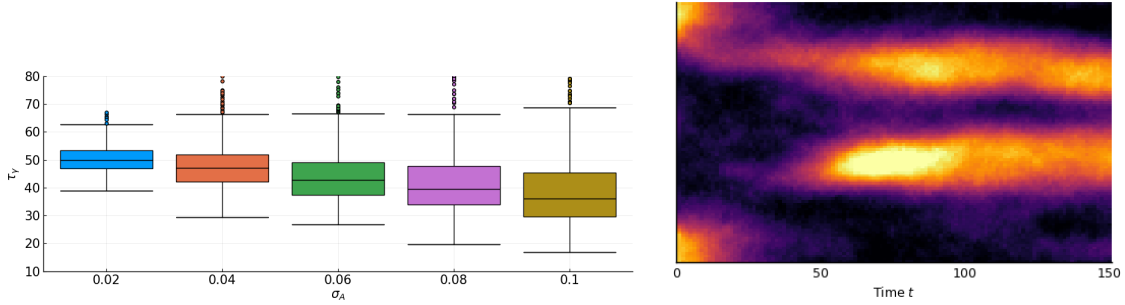


**Figure 2:** (left) Boxplots for the distribution of the time to repolarisation  $\tau_\gamma$  for different noise levels  $\sigma_A$ ; (right) a typical realisation of the stochastic Meinhardt model with larger noise level 0.05.

**Noise speeds up repolarisation** In Figure 1(center) we see the solution of (1) starting from a polarised state with high activator concentration in some part of the cell called 'rear'. Stimulated by the extracellular signal (3) the activator breaks down in order to reappear in an area of high signal strength called 'front', and the cell repolarises. Figure 1(right), on the other hand, contains a typical realisation of the SPDE (1). The evolution of activator concentration deviates considerably from the deterministic dynamics, but repolarisation is still achieved. For a more quantitative analysis consider the relative activator concentrations

$$\mu_F(t) = \frac{2}{L} \int_{S_F} A(t, x) dx, \quad \mu_R(t) = \frac{2}{L} \int_{S_R} A(t, x) dx, \quad t \geq 0,$$

near the front  $S_F = [L/4, 3L/4]$  and the rear  $S_R = [0, L/4) \cup (3L/4, L]$ . With this we define the 'time to repolarisation'

$$\tau_\gamma = \inf\{t \geq 0 : \mu_F(t) \geq \gamma \mu_R(t)\}$$

as the time when the activator concentration in the front part is significantly higher than in the rear depending on a threshold  $\gamma > 1$ . We computed  $\tau_\gamma$  for 500 Monte Carlo iterations with  $\gamma = 1.2$  for different noise levels  $\sigma_A \in \{0.02, 0.04, \dots, 0.10\}$  (see Appendix B for details on the numerical setup). The corresponding boxplots describing the distribution of  $\tau_\gamma$  depending on  $\sigma_A$  is contained in Figure 2(left). We see that the mean of  $\tau_\gamma$  decreases for growing  $\sigma_A$ , while the variance increases. For example, while  $\tau_\gamma = 50.82$  in the deterministic case (i.e.,  $\sigma_A = 0$ ), it is  $\tau_\gamma = 40.12$  (on average) in the case  $\sigma_A = 0.10$ . A similar behaviour holds for varying  $\sigma_I$ . The same qualitative results were obtained for parameters and initial conditions different from the ones in Appendix B.

We can conclude that repolarisation is not only stable under noise, but it is even accelerated. The interpretation of this behaviour could be that the noise breaks symmetries, making the dynamics more 'turbulent' and therefore the creation of a new front is sped up.

In principle, the noise may act such that repolarisation is never achieved. In case of the noise levels for  $\sigma_A$  considered above, however, this was not an issue and only very few

realisations of  $X$  had to be discarded for computing  $\tau_\gamma$ . Moreover, realisations of (1), which would have led to negative concentrations of  $A$  or  $I$ , were not taken into account (even for  $\sigma_A = 0.1$  this concerned only 2.6% of all simulated paths).

**Splitting of the front** For the deterministic Meinhardt model it has been shown by [24] that the repolarised front may not be stable. Indeed, if the parameters, obtained from fitting data on the short timescales at which repolarisation typically occurs (120 sec), are used for long term simulations, then the front splits into several parts. This can be verified for the parameters in Appendix B: upon repolarisation, the front splits first into two parts (around time  $t = 200$ ) and then into three parts (around time  $t = 700$ ).

From Figure 2(right) we see, however, that the stochastic Meinhardt model with a larger noise level may lead to a sudden split into several fronts, and even a renewed polarisation of the rear. For very small noise levels (for example,  $\sigma_A = 0.01$ ) the front splitting into three fronts occurs much faster (around  $t = 400 - 500$  s) than in the deterministic system, while for larger noise levels this occurs even faster.

We want to note that front splitting is a common feature of amoeboid cell migration, allowing cells to explore their environment. It is visible in single cell data, e.g., Figure 3(right), but not in Figure 1(left), which corresponds to data averaged over several cells. Still, in strong signal gradients cells can move with a single front for long times ( $>10$  minutes) [25]. The Meinhardt model for long term simulations requires a smaller diffusivity  $D_I$ . When  $D_I$  was reduced by 25%, both deterministic and stochastic solutions produced a single stable front.

## 4 Parameter estimation

We derive an estimator  $\hat{D}_{A,\delta}$  of the diffusivity  $D_A$  from first principles and state its main properties. Let us assume that we can measure the activator  $A$  at  $M$  points  $x_k \in \Lambda$  for  $k = 1, \dots, M$  over a period of time  $[0, T]$ . Measurements usually correspond to fluorescence distributions (for example of actin in [25]) at the cell cortex and are obtained through microscopy. This means that every measurement necessarily has a minimal spatial resolution  $\delta > 0$  determined by the experimental setup. It can be described by a *local measurement* [3], that is, a linear functional

$$A_\delta(t, x_k) := A(t) * K_\delta(x_k) = \langle A(t), K_{\delta, x_k} \rangle, \quad 0 \leq t \leq T, \quad (4)$$

where  $\langle \cdot, \cdot \rangle$  denotes the  $L^2(\Lambda)$  inner product and  $*$  means convolution with respect to  $K_\delta(x) := \delta^{-1/2} K(\delta^{-1}x)$  for a compactly supported function  $K \in H^2(\mathbb{R})$ , the classical  $L^2$ -Sobolev space of order 2. Moreover,  $K_{\delta, x_k} := K_\delta(\cdot - x_k)$  corresponds to the point spread function in imaging systems. Particular examples for  $K$  are bump functions (see Section 5 below). The scaling by  $\delta^{-1/2}$  is irrelevant for the estimator, but normalizes  $K_{\delta, x_k}$  in  $L^2$ -norm, that is,  $\|K_{\delta, x_k}\| = \|K\|_{L^2(\mathbb{R})}$ , and eases the notation later. From (1) we find that

$A_\delta(t, x_k)$  satisfies

$$\frac{\partial}{\partial t} A_\delta(t, x_k) = D_A A_\delta^\Delta(t, x_k) + \langle f_A(X(t, \cdot), \cdot), K_{\delta, x_k} \rangle + \sigma_A \|K\|_{L^2(\mathbb{R})} \xi_{A, k}(t), \quad (5)$$

with scalar white noise (in time)  $\xi_{A, k}(t) = \langle \xi_A(t), K_{\delta, x_k} \rangle / \|K\|_{L^2(\mathbb{R})}$ , and where

$$A_\delta^\Delta(t, x_k) := \frac{\partial^2}{\partial x^2} A_\delta(t, x_k) = \left\langle A(t), \frac{\partial^2}{\partial x^2} K_{\delta, x_k} \right\rangle. \quad (6)$$

Neglecting the contribution of the nonlinear term in (5) leads to a parametric estimation problem for  $D_A$  with respect to the scalar processes  $(A_\delta(t, x_k))_{0 \leq t \leq T}$  for  $k = 1, \dots, M$ . The maximum-likelihood estimator can be obtained, in principle, by Girsanov's theorem [23], but this leads to a non-explicit filtering problem, as explained in [3] for the case  $M = 1$ . Instead, consider the modified likelihood with stochastic differentials  $dA_\delta(t, x_k)$  (in time)

$$\mathcal{L}_\delta(D_A) = \exp \left( \frac{D_A}{\sigma_A^2 \|K\|_{L^2(\mathbb{R})}} \sum_{k=1}^M \left( \int_0^T A_\delta^\Delta(t, x_k) dA_\delta(t, x_k) - \frac{D_A}{2} \int_0^T (A_\delta^\Delta(t, x_k))^2 dt \right) \right).$$

Maximising with respect to  $D_A$  and assuming that we have also measurements  $(A_\delta^\Delta(t, x_k))_{0 \leq t \leq T}$  at our disposal, leads to the *augmented MLE*

$$\hat{D}_{A, \delta} = \frac{\sum_{k=1}^M \int_0^T A_\delta^\Delta(t, x_k) dA_\delta(t, x_k)}{\sum_{k=1}^M \int_0^T (A_\delta^\Delta(t, x_k))^2 dt}. \quad (7)$$

Note that this extends the construction of [3] to more than one pair of local measurements. Equivalently,  $\hat{D}_{A, \delta}$  can be obtained formally (that is, neglecting the term independent of  $D_A$  in the quadratic expansion and interpreting  $\frac{\partial}{\partial t} A_\delta dt = dA_\delta$ ) as minimiser of the least squares contrast

$$D_A \mapsto \sum_{k=1}^M \int_0^T \left( \frac{\partial}{\partial t} A_\delta(t, x_k) - D_A A_\delta^\Delta(t, x_k) \right)^2 dt.$$

With Brownian motions  $W_k(t) = \int_0^t \xi_{A, k}(s) ds$  we obtain from (5) the basic error decomposition

$$\hat{D}_{A, \delta} = D_A + \mathcal{I}_\delta^{-1} \mathcal{R}_\delta + \sigma_A \|K\|_{L^2(\mathbb{R})} \mathcal{I}_\delta^{-1} \mathcal{M}_\delta, \quad (8)$$

$$\text{with } \mathcal{I}_\delta = \sum_{k=1}^M \int_0^T (A_\delta^\Delta(t, x_k))^2 dt, \quad (\text{observed Fisher information})$$

$$\mathcal{M}_\delta = \sum_{k=1}^M \int_0^T A_\delta^\Delta(t, x_k) dW_k(t), \quad (\text{martingale part})$$

$$\mathcal{R}_\delta = \sum_{k=1}^M \int_0^T A_\delta^\Delta(t, x_k) \langle f_A(X(t, \cdot), \cdot), K_{\delta, x_k} \rangle dt. \quad (\text{nonlinear bias})$$



For  $M = 1$  and linear SPDEs with Dirichlet boundary conditions [3] show that  $\mathcal{I}_\delta \rightarrow \infty$  in probability for resolution  $\delta \rightarrow 0$ . We will see that this remains true in the present case with periodic boundary conditions and fixed  $M$ . For independent Brownian motions  $W_k$ , for example when the  $K_{\delta, x_k}$  have disjoint supports, the observed Fisher information  $\mathcal{I}_\delta$  corresponds to the quadratic variation of the martingale part  $\mathcal{M}_\delta$ . Consistency of  $\hat{D}_{A, \delta}$  is therefore expected to hold as soon as the nonlinear bias is not too large. For a nonlinearity depending only on the underlying process, that is  $A$ , [2] prove that this depends on its spatial regularity, but in our case  $f_A(X(t, \cdot), \cdot)$  also depends on additional randomness through the inhibitor  $I$ .

We prove in Appendix A.2 for fixed  $T$  and  $M$  that  $\hat{D}_{A, \delta}$  is not only a consistent estimator of  $D_A$  for resolution levels  $\delta \rightarrow 0$ , but also that its error satisfies a central limit theorem with rate  $\delta$  (which is optimal already for the linear case in [3]) and with explicit asymptotic variance.

**Theorem 2.** *Consider the setting of Theorem 1 and let  $K \in H^2(\mathbb{R})$  have compact support such that  $\|\frac{\partial}{\partial x} K\|_{L^2(\mathbb{R})} \neq 0$ . If  $\sigma_A > 0$ , then, as  $\delta \rightarrow 0$ ,  $\hat{D}_{A, \delta}$  is a consistent and asymptotically normal estimator of  $D_A$ , that is,*

$$\delta^{-1} \left( \hat{D}_{A, \delta} - D_A \right) \xrightarrow{d} N \left( 0, D_A \frac{\Sigma}{MT} \right), \quad \Sigma = \frac{2\|K\|_{L^2(\mathbb{R})}^2}{\|\frac{\partial}{\partial x} K\|_{L^2(\mathbb{R})}^2}.$$

The asymptotic variance in Theorem 2 decreases for more observations  $M$  and for a growing time horizon  $T$ , but is independent of the noise level  $\sigma_A$ , the initial value, the nonlinearity  $f_A$  and the inhibitor  $I$ . This robustness is particularly important in modelling realistic nonlinear dynamics such as (1), which are subject to model uncertainties in parameters and even in the form of the equation. In fact, the proof reduces the estimation problem to the linear case with vanishing  $f_A$  and with zero initial value. This is possible, because the nonlinear bias is asymptotically for  $\delta \rightarrow 0$  of much smaller order than the martingale part in (8). The dependence on  $\delta$  is comparable to the presence of a zero order term in a linear SPDE as opposed to a first order linearity, that is, a transport term, which can induce an asymptotic bias [3].

**Remark 3.** While we focus in Theorem 2 on the stochastic Meinhardt model, the proof reveals that the theorem also applies to the SPDE (1) with general boundary conditions and arbitrary nonlinearities  $f_A, f_I$ , as long as the semigroup generated by the Laplacian on  $L^2(\Lambda)$  is self-adjoint, and as long  $t \mapsto f_A(X(t, \cdot), \cdot) \in C([0, T]; C(\Lambda))$ ,  $\tilde{A} \in C([0, T]; C^2(\Lambda))$   $\mathbb{P}$ -almost surely, where  $\tilde{A}$  corresponds to the perturbation process of  $A$  in Theorem 1. The proof does not depend explicitly on the underlying domain  $\Lambda$  and also applies, with small notational changes, to general (even unbounded) domains  $\Lambda \subseteq \mathbb{R}^d$  for  $d \geq 1$ . In this sense, Theorem 2 generalises considerably similar results in [3], [2] for parametric diffusivity and spatially homogeneous noise. Moreover, the proof is self-contained and significantly shorter.

**Remark 4.** It is interesting to note that the robustness of the estimator  $\hat{D}_{A,\delta}$  to nonlinear perturbations  $f_A$  is an impact of the driving noise process. If there is no noise, that is,  $\sigma_A = \sigma_I = 0$ , then  $A(t) \in C^2(\Lambda)$ ,  $f_A(X(t, \cdot), \cdot) \in C(\Lambda)$  by classical theory for parabolic PDEs [14] or argue as in the proof of Theorem 1, which does not assume nonvanishing noise. This implies by convolution approximation uniformly in  $0 \leq t \leq T$  as  $\delta \rightarrow 0$

$$\begin{aligned} \langle f_A(X(t, \cdot), \cdot), \delta^{-1/2} K_{\delta, x_k} \rangle &\rightarrow f_A(X(t, x_k), x_k) \int_{\mathbb{R}} K(x) dx, \\ \delta^{-1/2} A_{\delta}^{\Delta}(t, x_k) &= \left\langle \frac{\partial^2}{\partial x^2} A(t, \cdot), \delta^{-1/2} K_{\delta, x_k} \right\rangle \rightarrow \frac{\partial^2}{\partial x^2} A(t, x_k) \int_{\mathbb{R}} K(x) dx. \end{aligned}$$

From this and the basic error decomposition (8) it follows then, assuming  $\int_{\mathbb{R}} K(x) dx \neq 0$  and  $\frac{\partial^2}{\partial x^2} A(t, x_k) \neq 0$  for at least on  $x_k$ , that  $\hat{D}_{A,\delta} - D_A$  converges to a non-zero constant. On the other hand, in the linear PDE case with  $f_A = 0$  and with  $\sigma_A = \sigma_I = 0$ , we have exactly  $\hat{D}_{A,\delta} = D_A$  and there is no estimation error.

As a consequence of Theorem 2 we can easily construct asymptotic confidence intervals for  $D_A$ .

**Corollary 5.** *Consider the setting of Theorem 2. For  $0 < \alpha < 1$ , confidence intervals  $I_{1-\alpha}$  and  $\tilde{I}_{1-\alpha}$  for  $D_A$  with asymptotic coverage  $1 - \alpha$  as  $\delta \rightarrow 0$  are given by*

$$\begin{aligned} I_{1-\alpha} &= \left[ \hat{D}_{A,\delta} - \frac{\delta}{(MT)^{1/2}} \left( \hat{D}_{A,\delta} \Sigma \right)^{1/2} q_{1-\alpha/2}, \hat{D}_{A,\delta} + \frac{\delta}{(MT)^{1/2}} \left( \hat{D}_{A,\delta} \Sigma \right)^{1/2} q_{1-\alpha/2} \right], \\ \tilde{I}_{1-\alpha} &= \left[ \hat{D}_{A,\delta} - \frac{\sigma_A \|K\|_{L^2(\mathbb{R})}}{\mathcal{I}_{\delta}^{1/2}} q_{1-\alpha/2}, \hat{D}_{A,\delta} + \frac{\sigma_A \|K\|_{L^2(\mathbb{R})}}{\mathcal{I}_{\delta}^{1/2}} q_{1-\alpha/2} \right], \end{aligned}$$

with the standard normal  $(1 - \alpha/2)$ -quantile  $q_{1-\alpha/2}$ .

While asymptotic coverage of the first confidence interval follows immediately from Slutsky's Lemma and Theorem 2, the statement with respect to  $\tilde{I}_{1-\alpha}$  is obtained from the error decomposition (8) and Proposition 6(i,ii,iii) below. Moreover, the confidence interval  $I_{1-\alpha}$  requires knowledge of  $K$  in form of  $\Sigma$  from Theorem 2, but the computation of  $\tilde{I}_{1-\alpha}$  is entirely data driven, based on the observed Fisher information  $\mathcal{I}_{\delta}$  and noting that the quadratic variation  $T\sigma_A^2 \|K\|_{L^2(\mathbb{R})}^2$  in (5) is identified from observing the trajectories of  $(A_{\delta}(t, x_k))_{0 \leq t \leq T}$  in continuous time.

## 5 Application to synthetic data

Let us apply the results of the previous section to the estimation of the diffusion constant  $D_A$ . Synthetic data of local measurements are obtained by simulating the SPDE (1) using a finite difference scheme as explained in Appendix B with experimentally calibrated  $D_A =$

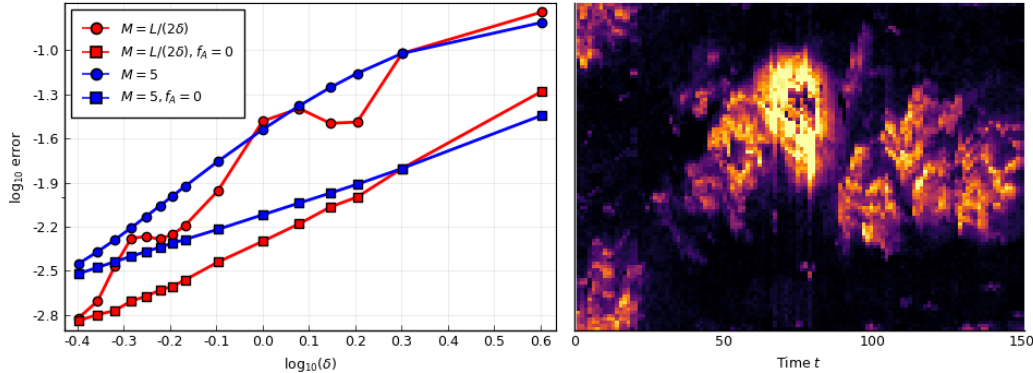


**Figure 3:** (left)  $\log_{10}$ - $\log_{10}$  plot of root mean squared estimation errors for different  $M$  with  $f_A$  and  $A_0$  calibrated to experimental data and in the linear case with  $f_A = 0$  and zero initial condition  $A_0$ ; (right) heatmap for 100 measurements of the activator along the cell contour for a single cell.

$4.415 \times 10^{-2}$ ,  $\sigma_A = 0.02$  and  $\sigma_I = 0$ . As a typical example for the kernel  $K$  we use the bump function

$$K(x) = \exp\left(-\frac{10}{1-x^2}\right) \mathbf{1}_{[-1,1]}(x), \quad x \in \mathbb{R}. \quad (9)$$

For different resolutions  $\delta \in [L * 0.017, L * 0.1]$  and different  $M$ , local measurements  $A_\delta(t_j, x_k)$ ,  $A_\delta^\Delta(t_j, x_k)$  are obtained according to (4) and (6) on regular grids  $x_k = Lk/M$ ,  $k = 0, \dots, M-1$ ,  $t_j = Tj/N$ ,  $j = 0, \dots, N$ . For these local measurements, the augmented MLE  $\hat{D}_{A,\delta}$  is computed.

Figure 3(left) shows a  $\log_{10}$ - $\log_{10}$  plot of root mean squared estimation errors obtained after 500 Monte Carlo iterations for  $T = 30$ ,  $L = 20$ ,  $m = 2000$  points in space and  $n = m^2/4$  points in time, with  $N = n/100$ . We show results for two different choices of  $M$ , namely fixed at  $M = 5$  for all  $\delta$ , and  $M \equiv M(\delta) = L/(2\delta)$ . In both cases, the supports of the kernels  $K_{\delta, x_k}$  are non-overlapping. For comparison, we also added root mean squared estimation errors for the linear SPDE with  $f_A = 0$  and with zero initial value  $A_0 = 0$ . The estimation errors are significantly smaller in the linear case, for both choices of  $M$ , therefore demonstrating clearly a strong non-asymptotic effect of the nonlinearity and the initial value. This difference disappears as  $\delta \rightarrow 0$ . In the linear case, the errors are very well aligned with the asymptotic standard error (when multiplied with  $\delta$ ) as predicted by Theorem 2. This allows us to read off the rates of convergence from the  $\log_{10}$ - $\log_{10}$  plots: for fixed  $M$  the rate of convergence is  $\delta$ , and for  $M(\delta) = L/(2\delta)$  it is approximately  $\delta/\sqrt{M} \approx \delta^{3/2}$ . These rates are not attained yet for the considered range of  $\delta$  with non-vanishing  $f_A$  and with a non-zero initial value. Note that for  $\delta = L * 0.017$  we only obtain  $M(\delta) = 30$  non-overlapping local measurements, whereas in the real-data example in the next section we have a much smaller  $\delta$  and 100 measurements. Finer simulations require significantly more computational efforts.

We have also verified the confidence intervals  $I_{1-\alpha}$  and  $\tilde{I}_{1-\alpha}$  of Corollary 5 empirically for different  $\alpha$ . For small  $\delta$ ,  $\tilde{I}_{1-\alpha}$  is always very close to, but slightly smaller than  $I_{1-\alpha}$  with better results for  $M(\delta)$  than for fixed  $M$  for both confidence intervals. We therefore focus now only on  $M(\delta)$  and  $I_{1-\alpha}$ . In the linear case coverage near the nominal level is obtained for all  $\delta$ . In the nonlinear case, good coverage requires relatively small  $\delta$ , but is always worse than for the linear case. For example, for  $\delta = L * 0.017$  and  $\alpha = 0.1$ ,  $I_{90}$  covers  $D_A$  only for 85% of the samples, and for  $\alpha = 0.05$  with  $I_{95}$  this increases to 92%. In one sample, with  $D_A$  was estimated at  $4.372 \times 10^{-2}$  with confidence bounds  $\pm 0.162 \times 10^{-2}$  according to  $I_{90}$ , and with  $\pm 0.193 \times 10^{-2}$  according to  $I_{95}$ . The confidence intervals are generally significantly smaller than in the linear case. Moreover, we have noticed that a larger time horizon  $T$  decreases the overall estimation errors, as predicted by Theorem 2, but coverage is noticeably worse in the nonlinear case, but still improves for smaller  $\delta$ , while performance is essentially unaffected in the linear case.

Further unreported simulations show that pointwise estimation results, that is, with  $M = 1$ , are not homogeneous in space, and are affected adversely at locations  $x_k$  where repolarisation leads to fast changes in the activator  $A$  (cf. Figure 1). This effect becomes smaller as  $\delta \rightarrow 0$ , because the nonlinearity plays no role in the asymptotic error according to Theorem 2. While the augmented MLE can account for these local fluctuations, we have noticed that the spectral estimator [18], obtained from a discrete Fourier transform of the local measurements, is affected considerably, and does not perform well, unless the number of measurements  $M$  is increased significantly. This leads, however, to overlapping supports of the  $K_{\delta, x_k}$ , which may not be realistic in experimental data, for example in case of the imaging data in the next section. For more details and different aspects of parameter estimation in reaction-diffusion equations using the spectral estimator see [31] in a related application to cell motility.

## 6 Application to experimental data

In this section we apply the augmented MLE to the experimental data described in Appendix B, that is to single cell data from 18 different single cells. Figure 3(right) shows the heatmap for one such cell. Compared to the average over these 18 cells in Figure 1(left), the activator behaves much more random, with cell fronts forming and disappearing quickly.

We assume that each data point corresponds to a local measurement  $A_\delta(t_j, x_k)$  for  $x_k = Lk/M$ ,  $k = 0, \dots, M - 1$  for  $M = 100$  and with  $t_j = Tj/N$ ,  $j = 0, \dots, N$ . Here,  $T = N$  ranges from 30 to 256 for different cells and we choose  $L = 20$ , as above. Using (6),  $A_\delta^\Delta(t_j, x_k)$  is computed by a finite difference approximation of the second derivative. This yields an approximated version of the augmented MLE  $\hat{D}_{A, \delta}$ . The confidence interval  $\tilde{I}_{1-\alpha}$  from Corollary 5 is obtained from the observed Fisher information, based on the

approximated  $A_\delta^\Delta(t_j, x_k)$ , and using the averaged realised variations

$$RV = M^{-1} \sum_{k=0}^{M-1} \sum_{j=1}^N (A_\delta(t_j, x_k) - A_\delta(t_{j-1}, x_k))^2,$$

to approximate the quadratic variation  $T\sigma_A^2 \|K\|_{L^2(\mathbb{R})}^2$ .

For the single cell data displayed in Figure 3(right) with  $T = 150$  we estimate  $D_A$  at  $1.605 \times 10^{-2} (\pm 0.022 \times 10^{-2})$ . Across the 18 cells the estimates are quite stable, the mean estimated diffusivity is  $1.773 \times 10^{-2}$ , with standard deviation  $0.176 \times 10^{-2}$ . These results remain essentially unchanged for smaller values of  $T$ . We have also applied the augmented MLE directly to the averaged data from Figure 1(left), yielding  $1.702 \times 10^{-2} (\pm 0.0258 \times 10^{-2})$  as estimate for  $D_A$ , implying that the estimator is robust to the averaging. Our estimates are of the same order as the ones from [25], who fitted the same data to the deterministic Meinhardt model using a least squares (profile likelihood) approach. Interestingly, they obtained  $4.415 \times 10^{-2}$  for  $D_A$  in case of the averaged data, but their estimates for the single cell data yield much smaller diffusivities, while our results are not affected much. We want to remark that our estimates are also of the same order as previously reported results in the literature in a comparable setup [15].

The time to repolarisation in the 18 cells (i.e,  $\tau_\gamma$  with  $\gamma = 1.2$ ) ranges from 16 to 51 with mean 23.83, which is a reasonable value for *Dictyostelium* cells. We have also simulated the stochastic Meinhardt model using the averaged estimated diffusivities, keeping the same parameters for  $f_A$  and the same initial conditions as in Section 5, and computed the time to repolarisation as in Section 3. The behaviour of  $\tau_\gamma$  is similar, with its mean decreasing for growing  $\sigma_A$ . For example, for  $\gamma = 1.2$ , we get  $\tau_\gamma = 51.34$  in the deterministic case,  $\tau_\gamma = 46.95$  (on average) when  $\sigma_A = 0.02$  and  $\tau_\gamma = 29.41$  (on average) for  $\sigma_A = 0.10$ . Since the estimated diffusivities are smaller than the diffusivity used for our previous simulations, several new fronts were typically built upon repolarisation. However, as discussed in Section 3, the reduction of  $D_I$  helps to create one stable front again.

## 7 Discussion

We have extended parameter estimation methods developed for linear SPDEs to systems of stochastic reaction-diffusion equations with periodic boundary conditions. The inclusion of noise into biological models is becoming increasingly relevant, owing to availability of high resolution measurement devices and improved computational methods.

As a concrete application we have estimated the diffusivity in a stochastic Meinhardt model for cell repolarisation. The estimator performed well on synthetic data and provided reasonable estimates across measurements for 18 single cells. For the considered SPDE model, we have demonstrated through simulations that moderate levels of dynamic noise do not destroy the pattern formation mechanism, but amplify it, leading to faster repolarisation

and front splitting. This is achieved despite the simple activator-inhibitor structure of (1) and using only space-time white noise. We believe that this is the starting point for studying more detailed models for cell repolarisation based on SPDEs with spatially nonhomogeneous and possibly multiplicative noise. In this way we hope to obtain models that recover the variations within cells and between different cell populations better.

The estimation methods developed here are not limited to the specific SPDE model under consideration, but can also be applied to other models for cell motility such as [15, 31], and even to general systems of stochastic reaction-diffusion equations under regularity conditions for the nonlinearity. This flexibility will be essential in calibrating SPDE models to experimental data.

## A Proofs

In the following, we consider for fixed  $T < \infty$  a filtered probability space  $(\Omega, \mathcal{F}, (\mathcal{F}_t)_{0 \leq t \leq T}, \mathbb{P})$ . Unless stated otherwise, all limits are taken as  $\delta \rightarrow 0$ .  $C$  always denotes a generic positive constant which may change from line to line.  $A \lesssim B$  means  $A \leq CB$  and  $A_n = \mathcal{O}_{\mathbb{P}}(B_n)$  means that  $A_n/B_n$  is tight, that is,  $\sup_n \mathbb{P}(|A_n| > C|B_n|) \rightarrow 0$  as  $C \rightarrow \infty$ . Recall that  $z \in L^p(\Lambda) = L^p(\Lambda; \mathbb{R})$  for  $p \geq 1$  and  $\Lambda = \mathbb{R}/(L\mathbb{Z})$  means  $z$  is  $L$ -periodic and  $z \in L^p([0, L])$ . We also write  $\Delta = \partial^2/\partial x^2$  to denote the Laplacian on  $L^2(\Lambda)$  with periodic boundary conditions.

### A.1 Existence of a unique solution

**Reformulation and mild solution** Let us first reformulate the Meinhardt model as an SPDE in the space  $L^2(\Lambda; \mathbb{R}^2)$ . Let  $S_A$  and  $S_I$  denote the analytic and self-adjoint semigroups generated by  $D_A\Delta$  and  $D_I\Delta$  on  $L^2(\Lambda)$ , cf. [4, Section 2.3]. For smooth  $z = (z_1, z_2) \in L^2(\Lambda; \mathbb{R}^2)$  consider also the differential operator  $\mathcal{A}z = (D_A\Delta z_1, D_I\Delta z_2)$  with periodic boundary conditions, generating the semigroup  $S(t)z = (S_A(t)z_1, S_I(t)z_2)$  on  $L^2(\Lambda; \mathbb{R}^2)$ . Let  $B : L^2(\Lambda; \mathbb{R}^2) \rightarrow L^2(\Lambda; \mathbb{R}^2)$ ,  $Bz = (\sigma_A z_1, \sigma_I z_2)$  and define  $F : L^2(\Lambda; \mathbb{R}^2) \rightarrow L^2(\Lambda; \mathbb{R}^2)$  by

$$F(z)(x) = (F_A(z)(x), F_I(z)(x)) = (f_A(z(x), x), f_I(z(x), x)).$$

Consider two independent cylindrical Wiener processes  $W_A, W_I$  on  $L^2(\Lambda)$  such that  $W(t) = (W_A(t), W_I(t))$  is a cylindrical Wiener process on  $L^2(\Lambda; \mathbb{R}^2)$ , and formally  $dW(t) = (\xi_A(t), \xi_I(t))dt$ . Solving (1) then corresponds to finding a solution  $X = (A, I)$  in  $L^2(\Lambda; \mathbb{R}^2)$  to the SPDE

$$\begin{cases} dX(t) = (\mathcal{A}X(t) + F(X(t))) dt + B dW(t), & 0 < t \leq T, \\ X(0) = (A_0, I_0). \end{cases} \quad (10)$$

We use the mild solution concept of [12]. We will show that there exists a process  $X$  taking values in  $L^2(\Lambda; \mathbb{R}^2)$  satisfying

$$X(t) = S(t)X(0) + \int_0^t S(t-s)F(X(s))ds + \int_0^t S(t-s)BdW(s). \quad (11)$$

**Linear and nonlinear parts** The idea is to obtain the existence of  $X$  from  $X := \bar{X} + \tilde{X}$  with the stochastic convolution  $\bar{X}(t) := \int_0^t S(t-s)BdW(s)$  and where  $\tilde{X}$  satisfies

$$\tilde{X}(t) = S(t)X(0) + \int_0^t S(t-s)F(\bar{X}(s) + \tilde{X}(s))ds, \quad 0 \leq t \leq T. \quad (12)$$

The process  $\bar{X}$  is the unique mild solution to the linear SPDE (10) (with  $F \equiv 0$  and  $X(0) = 0$ ) and takes values in  $L^2(\Lambda; \mathbb{R}^2)$  (apply, for example, [12, Theorem 5.4] separately to the component processes  $\bar{A}, \bar{I}$ ). Finding a process  $\tilde{X}$  solving (12), on the other hand, means equivalently finding a solution to the nonlinear PDE with random coefficients

$$\frac{\partial}{\partial t} \tilde{X}(t) = \mathcal{A}\tilde{X}(t) + F(\bar{X}(t) + \tilde{X}(t)), \quad 0 < t \leq T, \quad \tilde{X}(0) = X(0). \quad (13)$$

Since this equation does not depend explicitly on the noise process  $W$  anymore, it can be solved for a fixed realisation of  $\bar{X}$ . The proof follows from a classical fixed point argument.

*Proof of Theorem 1.* We first show that the linear process  $\bar{X}$  takes values in  $C^{s'}(\Lambda; \mathbb{R}^2)$ ,  $0 < s' < 1/2$ . For  $r \in \mathbb{R}$ ,  $p \geq 1$  consider the Bessel potential spaces on the 1D-torus  $\Lambda = \mathbb{R}/(L\mathbb{Z})$

$$W^{r,p}(\Lambda) := \{u \in L^p(\Lambda) : \|u\|_{r,p} < \infty\},$$

with norm  $\|u\|_{r,p} = \|(I - \Delta)^{r/2}u\|_{L^p(\Lambda)}$  [34, 10]. Note that  $I - \Delta$  is a strictly positive operator and thus  $(I - \Delta)^{-1}$  is a bounded operator on  $L^p(\Lambda)$  for periodic boundary conditions, while  $(-\Delta)^{-1}$  is not. The Bessel potential spaces differ from the classical Sobolev spaces, but allow for a Sobolev embedding theorem (see for example [10, Section 2.3] or [34]). We can now apply [2, Proposition 30] to conclude that  $\bar{A}, \bar{I} \in C([0, T]; W^{s',p}(\Lambda))$  for all  $0 < s' < 1/2$  and  $p \geq 2$  for the component processes of  $\bar{X}$ . Note that the proposition is stated for the Bessel potential spaces with respect to the Dirichlet Laplacian, but the statement and its proof remain true using the corresponding spaces defined above. Since  $p$  is arbitrary, the Sobolev embedding applied componentwise gives  $\bar{X} \in C([0, T]; C^{s'}(\Lambda; \mathbb{R}^2))$  for all  $0 < s' < 1/2$ , as claimed.

By a fixed point argument [16, Theorem 6.4], noting that  $X(0) \in C(\Lambda; \mathbb{R}^2)$  and  $F$  is globally Lipschitz continuous from  $C(\Lambda; \mathbb{R}^2)$  to  $C(\Lambda; \mathbb{R}^2)$ , we conclude that (11) and (12) have unique solutions  $X$  and  $\tilde{X}$  in  $C([0, T]; C(\Lambda; \mathbb{R}^2))$ . In order to obtain the higher regularity of  $\tilde{X}$ , let us introduce the spaces

$$W^{r,p}(\Lambda; \mathbb{R}^2) := \{z \in L^p(\Lambda; \mathbb{R}^2) : \|z\|_{r,p} < \infty\},$$

where, abusing notation, for  $z \in L^p(\Lambda; \mathbb{R}^2)$  we also write  $\|z\|_{r,p} = (\|z_1\|_{r,p}^p + \|z_2\|_{r,p}^p)^{1/p}$ . We see from (12) for  $\eta < 2$ ,  $\varepsilon > 0$  and  $0 \leq t \leq T$  that

$$\begin{aligned} \|\tilde{X}(t)\|_{\eta,p} &\leq \|S(t)X(0)\|_{\eta,p} + \int_0^t \|S(t-r)F(X(r))\|_{\eta,p} dr \\ &\lesssim \|X(0)\|_{\eta,p} + \int_0^t (t-r)^{-1+\varepsilon/2} \|F(X(r))\|_{\eta-2+\varepsilon,p} dr. \end{aligned} \quad (14)$$

Since  $X$  takes values in  $C(\Lambda; \mathbb{R}^2)$ , it follows easily that the same holds for  $F(X(\cdot))$ . Choosing  $\varepsilon = 2 - \eta$  and observing that  $X(0) \in C^{2+s}(\Lambda; \mathbb{R}^2)$  for  $0 < s < 1/2$  therefore imply  $\sup_{0 \leq t \leq T} \|\tilde{X}(t)\|_{\eta,p} < \infty$ . Since this is true for all  $p \geq 2$ , the Sobolev embedding yields  $\tilde{X} \in C([0, T]; C^{\eta'}(\Lambda; \mathbb{R}^2))$  for all  $\eta' < 2$ . Applying  $F$  again shows  $F(X(\cdot)) \in C([0, T]; C^{s'}(\Lambda; \mathbb{R}^2))$  for all  $0 < s' < 1/2$  (recall the regularity of  $\tilde{X}$  from above), and therefore (e.g., by [34, Theorem 3.3.2])

$$\sup_{0 \leq r \leq T} \|F(X(r))\|_{s',p} \lesssim \sup_{0 \leq r \leq T} \|F(X(r))\|_{C^{s'}(\Lambda; \mathbb{R}^2)} < \infty$$

for all  $1/p < s'' < s' < 1/2$  and  $p > 2$ . Using this in (14) with  $s'' = s + \varepsilon < 1/2$  for sufficiently small  $\varepsilon > 0$  and with  $2 + s$  instead of  $\eta$ , we conclude at last  $\sup_{0 \leq t \leq T} \|\tilde{X}(t)\|_{2+s,p} < \infty$  and thus  $\tilde{X} \in C([0, T]; C^{2+s}(\Lambda; \mathbb{R}^2))$ , finishing the proof.  $\square$

## A.2 Results on parameter estimation

Since we are not considering Dirichlet boundary conditions, we cannot rely on the Feynman-Kac arguments of [3] and [2] to study the action of the semigroup generated by  $\Delta$  on  $K_{\delta, x_k}$ . The following proof avoids this issue, and also holds for more general boundary conditions. The proof is inspired by [2, Theorem 3], but is fully self-contained.

Consider the decomposition  $A = \bar{A} + \tilde{A}$  into linear and nonlinear parts  $\bar{A}$  and  $\tilde{A}$  according to Section A.1. With this we also set

$$\begin{aligned} \bar{A}_\delta^\Delta(t, x_k) &:= \langle \bar{A}(t), \Delta K_{\delta, x_k} \rangle = \sigma_A \left\langle \int_0^t S_A(t-s) dW_A(s), \Delta K_{\delta, x_k} \right\rangle \\ &= \sigma_A \int_0^t \langle S_A(t-s) \Delta K_{\delta, x_k}, dW_A(s) \rangle, \end{aligned} \quad (15)$$

as well as  $\tilde{A}_\delta^\Delta(t, x_k) = \langle \tilde{A}(t), \Delta K_{\delta, x_k} \rangle$ . We also use the linear observed Fisher information  $\bar{\mathcal{I}}_\delta = \sum_{k=1}^M \int_0^T (\bar{A}_\delta^\Delta(t, x_k))^2 dt$ .

*Proof of Theorem 2.* Using that  $\|K_{\delta, x_k}\| = \|K\|_{L^2(\mathbb{R})}$ , the basic error decomposition (8) can equivalently be written as

$$\delta^{-1}(\hat{D}_{A,\delta} - D_A) = (\delta^2 \mathcal{I}_\delta)^{-1} \delta \mathcal{R}_\delta + \sigma_A \|K\|_{L^2(\mathbb{R})} (\delta^2 \mathcal{I}_\delta)^{-1/2} (\mathcal{I}_\delta^{-1/2} \mathcal{M}_\delta).$$



The martingale part satisfies  $\mathcal{M}_\delta = \mathcal{M}_\delta(T)$ , where  $\mathcal{M}_\delta(t') = \sum_{k=1}^M \int_0^{t'} A_\delta^\Delta(t, x_k) dW_k(t)$  is a continuous martingale in  $t' \geq 0$  with respect to the natural filtration generated by the Brownian motions  $W_k$  as a sum of such martingales. Without loss of generality let the  $K_{\delta, x_k}$  have disjoint supports, which is true for sufficiently small  $\delta$ , since  $M$  is fixed. But then the processes  $W_k$  are independent and the quadratic variation of the martingale  $\mathcal{M}_\delta(t')$  at  $t' = T$  is exactly  $\mathcal{I}_\delta$ . By a classical time-change [21, Theorem 3.4.6] we can write  $\mathcal{M}_\delta = \bar{w}_{\mathcal{I}_\delta}$  for a Brownian motion  $(\bar{w}(t))_{t \geq 0}$ , possibly defined on an extension of the underlying probability space. We conclude from Proposition 6(i,ii,iii) that  $\mathcal{I}_\delta / \mathbb{E}[\bar{\mathcal{I}}_\delta] \rightarrow 1$  in probability and

$$\frac{\mathcal{M}_\delta}{\mathcal{I}_\delta^{1/2}} = \frac{\mathbb{E}[\bar{\mathcal{I}}_\delta]^{1/2}}{\mathcal{I}_\delta^{1/2}} \cdot \frac{\bar{w}_{\mathcal{I}_\delta}}{\mathbb{E}[\bar{\mathcal{I}}_\delta]^{1/2}} \xrightarrow{d} N(0, 1).$$

Proposition 6(i,ii,iii) also shows  $\delta^2 \mathcal{I}_\delta \rightarrow \kappa$  in probability and the result follows from Slutsky's Lemma and Proposition 6(iv).  $\square$

**Proposition 6.** *The following holds as  $\delta \rightarrow 0$ :*

- (i)  $\delta^2 \mathbb{E}[\bar{\mathcal{I}}_\delta] \rightarrow \kappa := MT\sigma_A^2 D_A^{-1} \|K\|_{L^2(\mathbb{R})}^2 \Sigma^{-1}$  with  $\Sigma$  from Theorem 2,
- (ii)  $\bar{\mathcal{I}}_\delta / \mathbb{E}[\bar{\mathcal{I}}_\delta] \rightarrow 1$  in probability,
- (iii)  $\mathcal{I}_\delta = \bar{\mathcal{I}}_\delta + \mathcal{O}_{\mathbb{P}}(\delta^{-1/2})$ ,
- (iv)  $\mathcal{R}_\delta = \mathcal{O}_{\mathbb{P}}(\delta^{-1/2})$ .

*Proof.* (i). We find from (15) and Itô's isometry ([12, Proposition 4.28]) that

$$\mathbb{E}[\bar{\mathcal{I}}_\delta] = \sigma_A^2 \sum_{k=1}^M \int_0^T \int_0^t \|S_A(s) \Delta K_{\delta, x_k}\|^2 ds dt. \quad (16)$$

The operators  $S_A(s)$  are self-adjoint such that  $\|S_A(s) \Delta K_{\delta, x_k}\|^2 = \langle S_A(2s) \Delta K_{\delta, x_k}, \Delta K_{\delta, x_k} \rangle$ . The semigroup identity  $2 \int_0^t S_A(2s) D_A \Delta K_{\delta, x_k} ds = S_A(2t) K_{\delta, x_k} - K_{\delta, x_k}$  therefore implies

$$\begin{aligned} \mathbb{E}[\bar{\mathcal{I}}_\delta] &= \frac{1}{2} D_A^{-1} \sigma_A^2 \sum_{k=1}^M \left( \int_0^T \langle S_A(2t) \Delta K_{\delta, x_k}, K_{\delta, x_k} \rangle dt - T \langle K_{\delta, x_k}, \Delta K_{\delta, x_k} \rangle \right) \\ &= \frac{1}{2} D_A^{-1} \sigma_A^2 \sum_{k=1}^M \left( \frac{1}{2} D_A^{-1} \langle S_A(2T) K_{\delta, x_k} - K_{\delta, x_k}, K_{\delta, x_k} \rangle - T \langle K_{\delta, x_k}, \Delta K_{\delta, x_k} \rangle \right). \end{aligned}$$

Noting that  $\|S_A(T) K_{\delta, x_k}\| \leq \|K_{\delta, x_k}\|$ , because the semigroup is contractive, (i) follows from  $\langle K_{\delta, x_k}, \Delta K_{\delta, x_k} \rangle = -\delta^{-2} \|\frac{\partial}{\partial x} K\|_{L^2(\mathbb{R})}^2$ .

(ii). It is enough to show  $\delta^4 \text{Var}(\bar{\mathcal{I}}_\delta) \rightarrow 0$ , because this and (i) imply  $\text{Var}(\bar{\mathcal{I}}_\delta) / \mathbb{E}[\bar{\mathcal{I}}_\delta]^2 \rightarrow 0$ . Since  $M$  is fixed, we can use the Cauchy-Schwarz inequality to obtain the upper bound

$\text{Var}(\bar{\mathcal{I}}_\delta) \leq M \sum_{k=1}^M \text{Var}(\int_0^T (\bar{A}_\delta^\Delta(t, x_k))^2 dt)$ . (15) shows that the  $\bar{A}_\delta^\Delta(t, x_k)$  are centered Gaussian random variables. Wick's formula ([19, Theorem 1.28]) gives

$$\begin{aligned} \text{Var}(\bar{\mathcal{I}}_\delta) &\lesssim \sum_{k=1}^M \int_0^T \int_0^T \text{Cov} \left( (\bar{A}_\delta^\Delta(t, x_k))^2, (\bar{A}_\delta^\Delta(t', x_k))^2 \right) dt' dt \\ &= 4 \sum_{k=1}^M \int_0^T \int_0^t \text{Cov} (\bar{A}_\delta^\Delta(t, x_k), \bar{A}_\delta^\Delta(t', x_k))^2 dt' dt \\ &= 4\sigma_A^4 \sum_{k=1}^M \int_0^T \int_0^t \left( \int_0^{t'} \langle S_A(t-s)\Delta K_{\delta, x_k}, S_A(t'-s)\Delta K_{\delta, x_k} \rangle ds \right)^2 dt' dt, \end{aligned}$$

again using Itô's isometry in the last line. Arguing as in (i) by the semigroup identity and  $S_A(t-s) = S_A(t-t')S_A(t'-s)$ , the  $ds$ -integral equals

$$\begin{aligned} &\int_0^{t'} \langle S_A(2(t'-s))\Delta K_{\delta, x_k}, S_A(t-t')\Delta K_{\delta, x_k} \rangle ds \\ &= \frac{1}{2D_A} \langle (S_A(2t') - I)K_{\delta, x_k}, S_A(t-t')\Delta K_{\delta, x_k} \rangle \leq \frac{1}{2D_A} \langle K_{\delta, x_k}, S_A(t-t')(-\Delta)K_{\delta, x_k} \rangle, \end{aligned}$$

where we used in the inequality that the  $-\Delta$  and thus  $S_A(t)$  for  $t \geq 0$  are self-adjoint, non-negative operators, which commute. This also shows that the  $ds$ -integral from above is in fact non-negative, and so we obtain from the last display using the Cauchy-Schwarz inequality

$$\text{Var}(\bar{\mathcal{I}}_\delta) \lesssim \|K\|_{L^2(\mathbb{R})}^2 \sum_{k=1}^M \int_0^T \int_0^t \|S_A(t')\Delta K_{\delta, x_k}\|^2 dt' dt \lesssim \mathbb{E}[\bar{\mathcal{I}}_\delta] \lesssim \delta^{-2},$$

cf. (16) and (i), implying  $\delta^4 \text{Var}(\bar{\mathcal{I}}_\delta) \rightarrow 0$  and (ii) follows.

(iii). Recall from Theorem 1 that  $\tilde{A} \in C([0, T]; C^2(\Lambda))$   $\mathbb{P}$ -almost surely. This means

$$\left| \tilde{A}_\delta^\Delta(t, x_k) \right| = \left| \langle \Delta \tilde{A}(t), K_{\delta, x_k} \rangle \right| \leq \|\tilde{A}\|_{C([0, T]; C^2(\Lambda))} \|K_{\delta, x_k}\|_{L^1(\Lambda)} = \mathcal{O}_{\mathbb{P}}(\delta^{1/2}), \quad (17)$$

using  $\|K_{\delta, x_k}\|_{L^1(\Lambda)} \leq \delta^{1/2} \|K\|_{L^1(\mathbb{R})}$ . We conclude by the Cauchy-Schwarz inequality and (i), because

$$|\mathcal{I}_\delta - \bar{\mathcal{I}}_\delta| \lesssim \sum_{k=1}^M \int_0^T \left( \left( \tilde{A}_\delta^\Delta(t, x_k) \right)^2 + 2 \left| \tilde{A}_\delta^\Delta(t, x_k) \bar{A}_\delta^\Delta(t, x_k) \right| \right) dt = \mathcal{O}_{\mathbb{P}}(\delta + \delta^{1/2} \bar{\mathcal{I}}_\delta^{1/2}).$$

(iv). The Cauchy-Schwarz inequality and (i,ii,iii) show

$$|\mathcal{R}_\delta| \lesssim \mathcal{I}_\delta^{1/2} \left( \sum_{k=1}^M \int_0^T \langle F_A(X(t)), K_{\delta, x_k} \rangle^2 dt \right)^{1/2} \lesssim \mathcal{I}_\delta^{1/2} \delta^{1/2} \|F_A(X(\cdot))\|_{C([0, T]; C(\Lambda))} \|K\|_{L^1(\mathbb{R})}.$$

This is of order  $\mathcal{O}_{\mathbb{P}}(\delta^{-1/2})$ , using that  $F_A(X(\cdot)) \in C([0, T]; C(\Lambda))$   $\mathbb{P}$ -almost surely by Theorem 1, recalling that  $z \mapsto F_A(z)$  is Lipschitz, and the result follows.  $\square$

## B Setup of numerical and real data experiments

Numerical simulations were performed in the programming language Julia using a finite difference scheme for semilinear SPDEs [26]. The source code can be obtained from the authors upon request. For comparison to the experimental setup of [25] we let  $L = 20$ ,  $T \in (0, 150]$ , and set  $dt = T/n$  and  $dx = L/m$  as step sizes for time and space discretisations, and choose the number of grid points  $n$  and  $m$  in time and space such that  $dt \asymp (dx)^2$ . This ensures that the Courant-Friedrichs-Lewy (CFL) condition is satisfied [26], in order to achieve stable simulations. All simulations were performed with parameters and initial conditions from [25] obtained by calibrating the deterministic Meinhardt model to the experimental data displayed in 1(left), which were averaged over 18 different cells. The parameters in (1), (2) and (3) are taken from [25, Table S1, Figure 4],

$$\begin{aligned} D_A &= 4.415 \times 10^{-2}, & D_I &= 9.768 \times 10^{-2}, \\ r_A &= 2.393 \times 10^{-1}, & r_I &= 2.378 \times 10^{-1}, \\ b_A &= 2.776 \times 10^{-1}, & b_I &= 2.076 \times 10^{-1}, \\ \zeta_A &= 5.647 \times 10^{-3}, & \zeta_I &= 3.397 \times 10^{-1}, \\ a &= 1.280 \times 10^{-2}. \end{aligned}$$

The initial conditions for the activator  $A$  and inhibitor  $I$  are taken correspondingly from [25, Table S2, Figure 4].

For the real data analysis in Section 6 data for the 18 single cells were used. They each contain  $M = 100$  spatial measurements for evolving over time. For a detailed description of the original experimental data see [13] and [24].

## References

- [1] Alonso, S., Stange, M., and Beta, C. (2018). Modeling random crawling, membrane deformation and intracellular polarity of motile amoeboid cells. *PLOS ONE*, 13(8):e0201977.
- [2] Altmeyer, R., Cialenco, I., and Pasemann, G. (2020). Parameter estimation for semi-linear SPDEs from local measurements. *arXiv preprint arXiv:2004.14728*.
- [3] Altmeyer, R. and Reiß, M. (2020). Nonparametric estimation for linear SPDEs from local measurements. *Annals of Applied Probability*, to appear.
- [4] Berglund, N. (2019). An introduction to singular stochastic PDEs: Allen-Cahn equations, metastability and regularity structures. *arXiv preprint arXiv:1901.07420*.
- [5] Bibinger, M. and Trabs, M. (2020). Volatility estimation for stochastic PDEs using high-frequency observations. *Stochastic Processes and their Applications*, 130(5):3005–3052.

- [6] Cheng, Y., Felix, B., and Othmer, H. G. (2020). The roles of signaling in cytoskeletal changes, random movement, direction-sensing and polarization of eukaryotic cells. *Cells*, 9(6):1437.
- [7] Chong, C. (2020). High-frequency analysis of parabolic stochastic PDEs. *Annals of Statistics*, 48(2):1143–1167.
- [8] Cialenco, I. (2018). Statistical inference for SPDEs: an overview. *Statistical Inference for Stochastic Processes*, 21(2):309–329.
- [9] Cialenco, I. and Huang, Y. (2019). A note on parameter estimation for discretely sampled SPDEs. *Stochastics and Dynamics*, 24:2050016.
- [10] Cirant, M. and Goffi, A. (2019). On the existence and uniqueness of solutions to time-dependent fractional MFG. *SIAM Journal on Mathematical Analysis*, 51(2):913–954.
- [11] Cramer, L. P. (2013). Mechanism of cell rear retraction in migrating cells. *Current opinion in cell biology*, 25(5):591–599.
- [12] Da Prato, G. and Zabczyk, J. (2014). *Stochastic equations in infinite dimensions*. Cambridge University Press.
- [13] Dalous, J., Burghardt, E., Müller-Taubenberger, A., Bruckert, F., Gerisch, G., and Bretschneider, T. (2008). Reversal of cell polarity and actin-myosin cytoskeleton reorganization under mechanical and chemical stimulation. *Biophysical journal*, 94(3):1063–1074.
- [14] Evans, L. C. (2010). *Partial Differential Equations*. American Mathematical Soc.
- [15] Fukushima, S., Matsuoka, S., and Ueda, M. (2019). Excitable dynamics of Ras triggers spontaneous symmetry breaking of PIP3 signaling in motile cells. *Journal of Cell Science*, 132(5).
- [16] Hairer, M. (2009). An Introduction to Stochastic PDEs. *arXiv preprint arXiv:0907.4178*.
- [17] Hildebrandt, F. and Trabs, M. (2019). Parameter estimation for SPDEs based on discrete observations in time and space. *arXiv preprint arXiv:1710.01649*.
- [18] Huebner, M. and Rozovskii, B. (1995). On asymptotic properties of maximum likelihood estimators for parabolic stochastic PDE's. *Probability Theory and Related Fields*, 103(2):143–163.
- [19] Janson, S. (1997). *Gaussian Hilbert Spaces*. Cambridge University Press.

- [20] Jilkinė, A. and Edelstein-Keshet, L. (2011). A comparison of mathematical models for polarization of single eukaryotic cells in response to guided cues. *PLoS Computational Biology*, 7(4):e1001121.
- [21] Karatzas, I. and Shreve, S. (1998). *Brownian Motion and Stochastic Calculus*. Springer.
- [22] Levchenko, A. and Iglesias, P. A. (2002). Models of eukaryotic gradient sensing: application to chemotaxis of amoebae and neutrophils. *Biophysical journal*, 82(1):50–63.
- [23] Liptser, R. and Shiryaev, A. (2001). *Statistics of Random Processes I. General Theory*. Springer.
- [24] Lockley, R. (2017). *Image-based Modelling of Cell Reorientation*. PhD thesis, University of Warwick.
- [25] Lockley, R., Ladds, G., and Bretschneider, T. (2015). Image based validation of dynamical models for cell reorientation. *Cytometry Part A*, 87(6):471–480.
- [26] Lord, G. J., Powell, C. E., and Shardlow, T. (2014). *An Introduction to Computational Stochastic PDEs*. Cambridge University Press.
- [27] Meinhardt, H. (1999). Orientation of chemotactic cells and growth cones: models and mechanisms. *Journal of cell science*, 112(17):2867–2874.
- [28] Meinhardt, H. (2009). *The algorithmic beauty of sea shells*. Springer.
- [29] Mullins, R. D., Heuser, J. A., and Pollard, T. D. (1998). The interaction of arp2/3 complex with actin: nucleation, high affinity pointed end capping, and formation of branching networks of filaments. *Proceedings of the National Academy of Sciences*, 95(11):6181–6186.
- [30] Otsuji, M., Ishihara, S., Kaibuchi, K., Mochizuki, A., and Kuroda, S. (2007). A mass conserved reaction-diffusion system captures properties of cell polarity. *PLoS Computational Biology*, 3(6):p. e108.
- [31] Pasemann, G., Flemming, S., Alonso, S., Beta, C., and Stannat, W. (2020). Diffusivity estimation for activator-inhibitor models: Theory and application to intracellular dynamics of the actin cytoskeleton. *arXiv preprint arXiv:2005.09421*.
- [32] Pasemann, G. and Stannat, W. (2020). Drift estimation for stochastic reaction-diffusion systems. *Electronic Journal of Statistics*, 14(1):547–579.
- [33] Spill, F., Guerrero, P., Alarcon, T., Maini, P. K., and Byrne, H. (2015). Hybrid approaches for multiple-species stochastic reaction–diffusion models. *Journal of computational physics*, 299:429–445.

- [34] Triebel, H. (2010). *Theory of Function Spaces*. Springer.
- [35] Turing, A. M. (1952). The chemical basis of morphogenesis. *Philosophical Transactions of the Royal Society of London. Series B, Biological Sciences*, 237(641):37–72.